Shallow P and S velocity structure, Red Deer, Alberta

Don C. Lawton, Meredith A. McArthur, Rachel T. Newrick and Sarah E. Trend

ABSTRACT

A multioffset vertical seismic profile was acquired at a site near Red Deer, Alberta, using a compressional minvibe source. A five-level, three-component VSP tool with a 15 m receiver spacing was used for data acquisition over a vertical aperture from surface to 300 m depth. First arrivals of offset data revealed the presence of turning rays for both P-waves and S-waves. Traveltimes and incident angles were inverted to yield a five-layer isotropic P-wave velocity model. P-wave velocity gradients of 10 s^{-1} and 5 s^{-1} were derived for the top two layers, respectively, and weak anisotropy ($\varepsilon = 0.02$ and $\delta = 0.02$) was deduced for the two shallowest layers. Direct S-waves were also recorded in the walk-away data. First-arrival traveltime and incident angle analysis yielded SV-wave velocity gradients up to18 s^{-1}.

INTRODUCTION

A multi-offset, multicomponent vertical seismic profile (VSP) was acquired at the Cygnet 9-34-38-28W4 lease, located Northwest of Red Deer, Alberta (Figure 1). At this location, enhanced coalbed methane production and carbon dioxide sequestration within the upper Cretaceous Ardley coal zone were to be evaluated. Unfortunately, initial tests showed low permeability within the coals and the site was ultimately abandoned. However, the VSP data acquired were very successful at imaging the Ardley coals and the zero-offset data were analyzed to determine the vertical P-wave and S-wave vertical velocity structure (Richardson and Lawton, 2003a). The current paper further investigates the shallow velocity structure from the analysis of the walkaway VSP data.

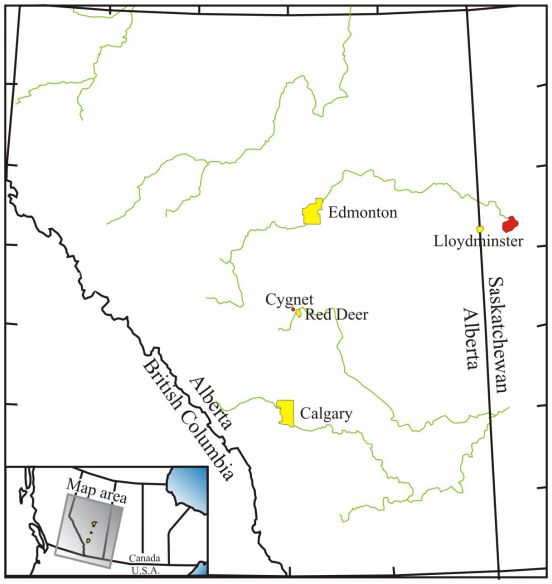

FIG. 1. Location of the Red Deer vertical seismic profile data set.

The Ardley coals are one of Alberta's most prospective natural gas from coal (NGC) targets. Ardley coal seams are unconformably overlain by the interbedded sands and shales of the Tertiary Paskapoo Formation, and underlain by Edmonton Group strata, of similar lithology to the Paskapoo (Figure 2). The Kneehills tuff (KH) forms an important regional marker bed within the Battle Formation, as it is an easily correlatable, laterally extensive layer containing volcanic ash, displaying low resistivity on well logs, and low seismic velocity (Havard et al., 1968).

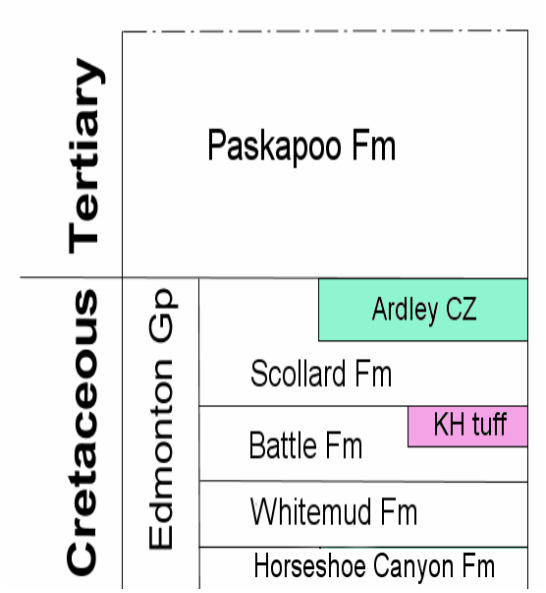

FIG. 2. Stratigraphic column showing Upper Cretaceous/Tertiary strata in Central Plains of Alberta (after Beaton, 2003).

Open-hole and cased hole logs from the Cygnet VSP well are shown in Figures 3 and 4 respectively. The Ardley coals occur at 290 m below KB and the overlying and underlying strata are interpreted as interbedded shales and siltstones, and three distinct Paskapoo sand units are identified in addition to the Ardley coal zone. The base of the well contains interbedded silts and shales. Overlying these strata is the Ardley coal zone, which is 11.7 m thick, from 282.3 m KB to 294.0 m depth. It is detectable on the well logs by its low density, as well as its low sonic velocity, and low gamma-ray response.

Strata overlying the Ardley coal zone belong to the Paskapoo Formation, which comprises interbedded fluvial sandstones and overbank shales (Smith, 1994). Three separate Paskapoo sand packages were identified by their low gamma-ray counts and relatively low sonic transit times. Sand C, with an upper contact at 272.0 m, immediately overlies the Ardley coal zone. Its gamma-ray profile is characteristic of a fining-upward fluvial sequence, with the cleanest gamma response at its base, becoming increasingly shaley towards the top. Its sharp contact with the underlying Ardley and its fluvial signature lead it to be interpreted as a channel sand.

Sand B is a thinner sedimentary package than sand C, being 8 m thick with an upper contact at 243.0 m. It is characterized by a clean, blocky gamma-ray signature. Sand B is interpreted to be a high-energy channel deposit.

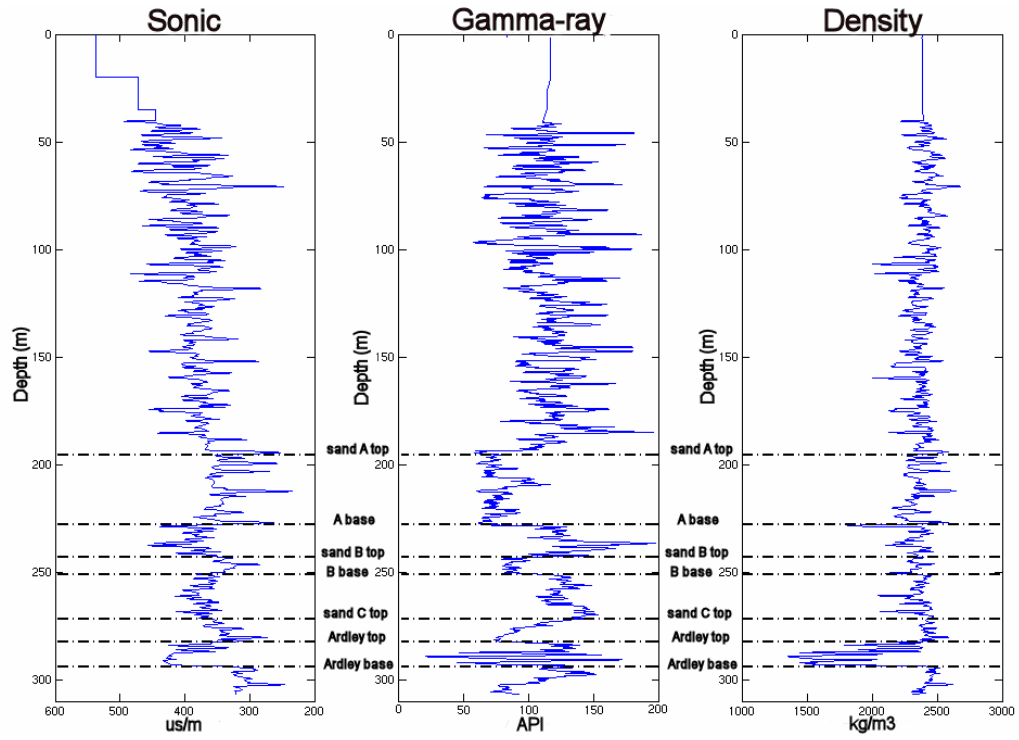

FIG. 3. P-wave sonic (left), gamma-ray (centre) and density (right) open-hole logs from the Cygnet VSP well.

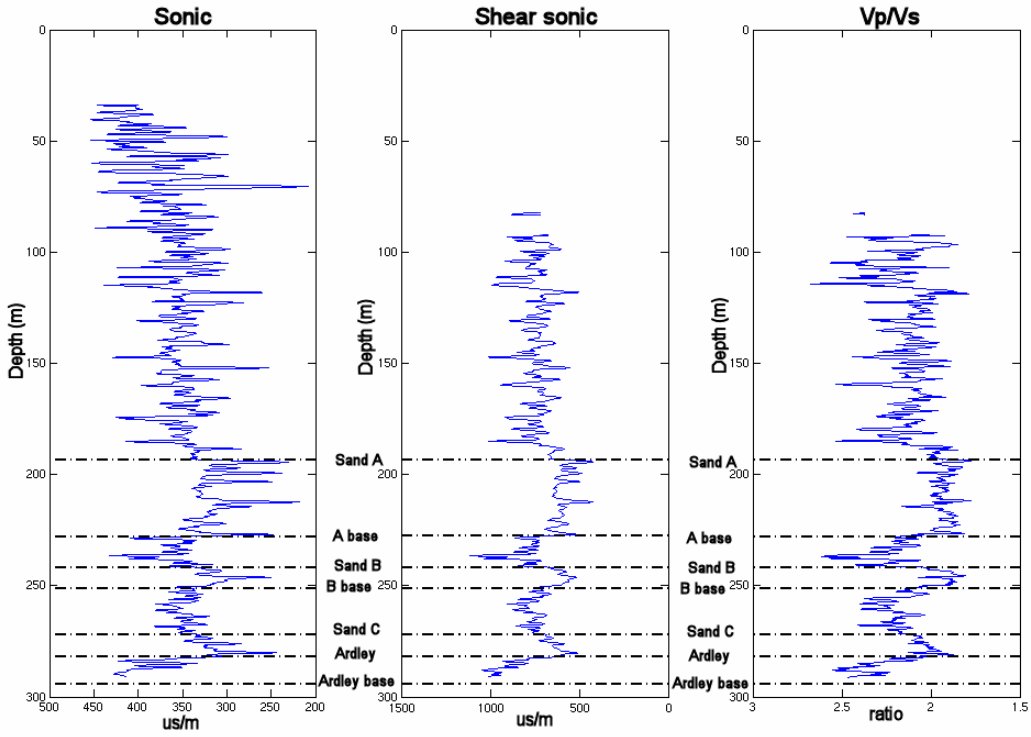

FIG. 4. P-wave (left), S-wave (centre) and gamma-ray (right) cased-logs from the Red Deer VCP well.

Sand A is 34.6 m thick, and is interpreted to start at 193.5 m KB with its basal contact at 228.1 m KB. The blocky log character with sharp upper and lower contacts suggests a well-sorted fluvial channel, typical of the Paskapoo Formation (Smith, 1994). A thin shaley layer (3-4 m thick) is noted in the middle of this sand body.

VSP DATA ACQUISITION

Receivers were located down the Cygnet well, from 20 m to 295 m depth, using a 5-level 3-component VSP tool with receivers spaced at 15 m intervals for the walk-away surveys. Source points were located at 20 m for the zero-offset survey, and at offsets of 100 m, 150 m, 191 m and 244 m, using a vertical minivibe source and 4 summed sweeps from 8 to 250 Hz, each over 8 seconds.

V_P/V_S ANALYSIS

Richardson and Lawton (2003a) reported on the analysis of the zero-offset VSP data, both in terms of imaging and Vp/Vs analysis. Figures 5 and 6 show a plot of average and interval Vp/Vs with depth, respectively.

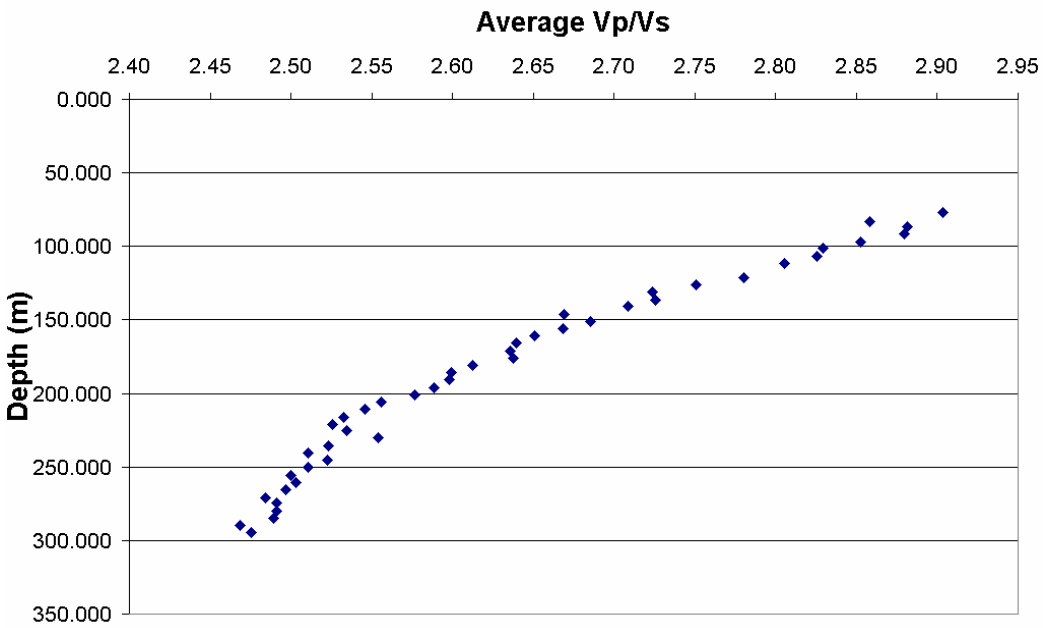

FIG. 5. Average Vp/Vs from analysis of the zero-offset VSP data at Cygnet

The data in Figures 5 shows a decreasing average Vp/Vs with depth, from a value of about 2.9 at 70 m depth, to about 2.4 at the base of the well. This trend is similar to that seen in other near-surface sediments in the Western Canada Sedimentary Basin and elsewhere.

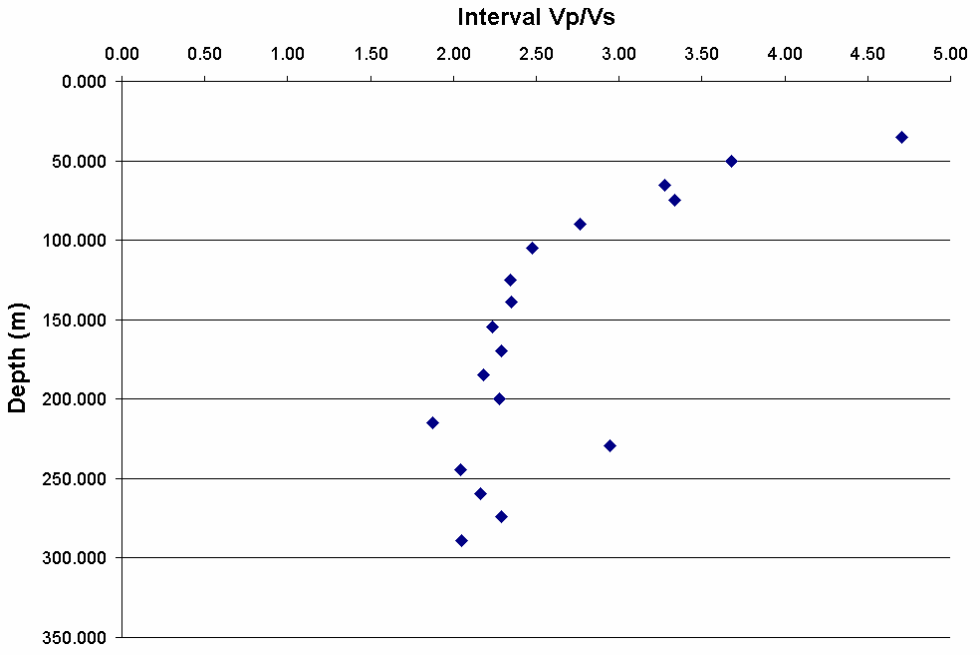

FIG. 6. Interval Vp/Vs from analysis of the zero-offset VSP data at Cygnet

Interval Vp/Vs values (Figure 6) are very high (greater than 4) in the near surface, decreasing to values of approximately 2.0 at depths greater than about 200 m. The Ardley coals have a Vp/Vs of approximately 2.4.

TURNING RAY ANALYSIS

Figure 7 shows the vertical component data from the VSP for the zero-offset shot (a) and the four offset shots (b through e). One receiver (at 115 m depth) had poor coupling and was edited from the records. The first arrival data in these shot gathers show several interesting features:

- The minimum first-arrival traveltime is observed deeper in the well with increasing source offset. At this depth, the apparent or vertical slowness changes sign, and we define this as the 'slowness cross-over depth'.
- The first arrivals show reversed polarity at depths shallower that that at which the minimum time is recorded.
- The moveout of the first arrivals at shallow depths is non-linear.

These observations are interpreted to be caused by turning rays in the shallow subsurface, caused by a vertical velocity gradient in the sediments. A P-wave velocity model was developed from the zero-offset and well-log data, including a gradient function of the form:

$$V(z) = Vo + kZ\,, \tag{1}$$

where Z is the depth below the top of a particular layer, k is the gradient and Vo is the velocity at the top of the layer.

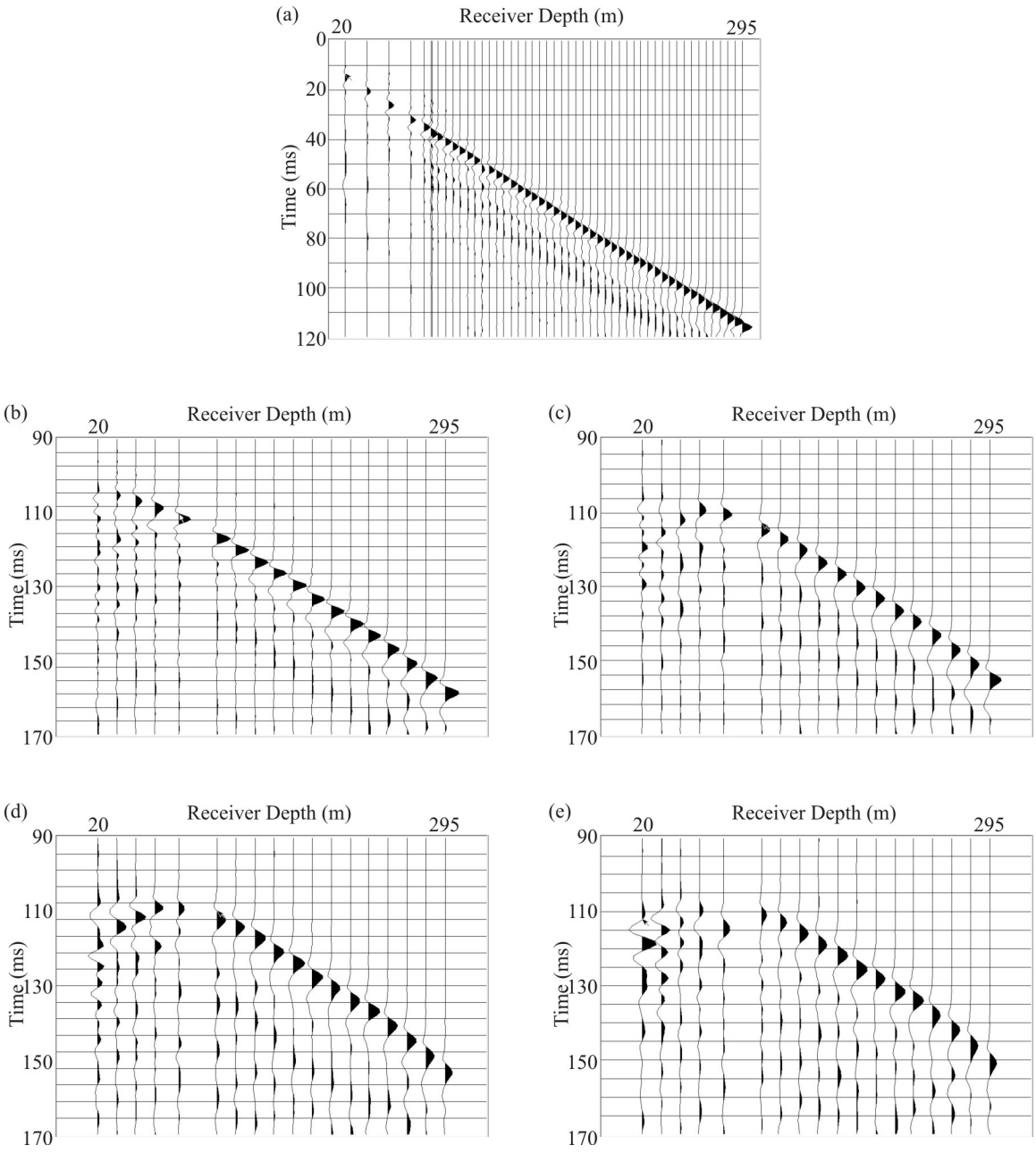

FIG. 7. Vertical-component of shot-gathers for source offsets of (a) 20 m, (b) 100 m, (c) 150 m, (d) 191 m and (e) 244 m. A polarity change with increasing depth is indicative of turning rays.

Raytracing was undertaken through the model to compare calculated and observed first-arrival traveltimes from each of the source offsets. Figure 8 shows an example of the ray geometry for the velocity model, with turning rays evident in the shallow part of the model. A linear increase in velocity with depth will result in raypaths that are circular arcs (Slotnick, 1959). At depths less than the slowness cross-over depth for each offset, the first arrival is upcoming energy, whereas at depths greater than the slowness cross-over depth, the first-arriving energy is down-going. This explains the polarity reversal on the vertical component data shown in Figure 7.

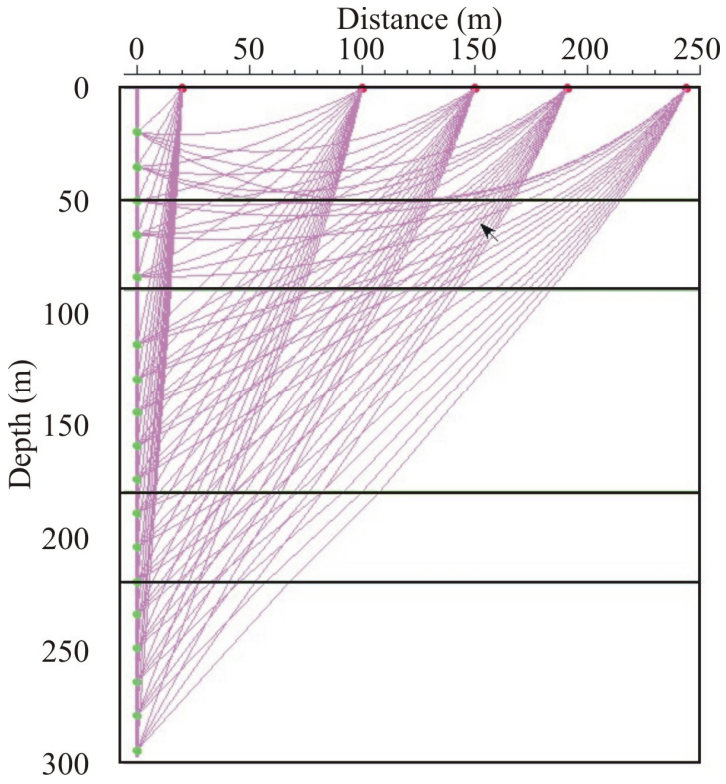

FIG. 8. Illustration of turning rays modelled the for Cygnet VSP dataset.

An isotropic model using was found to match computed and observed traveltimes well, as shown in Figure 9.

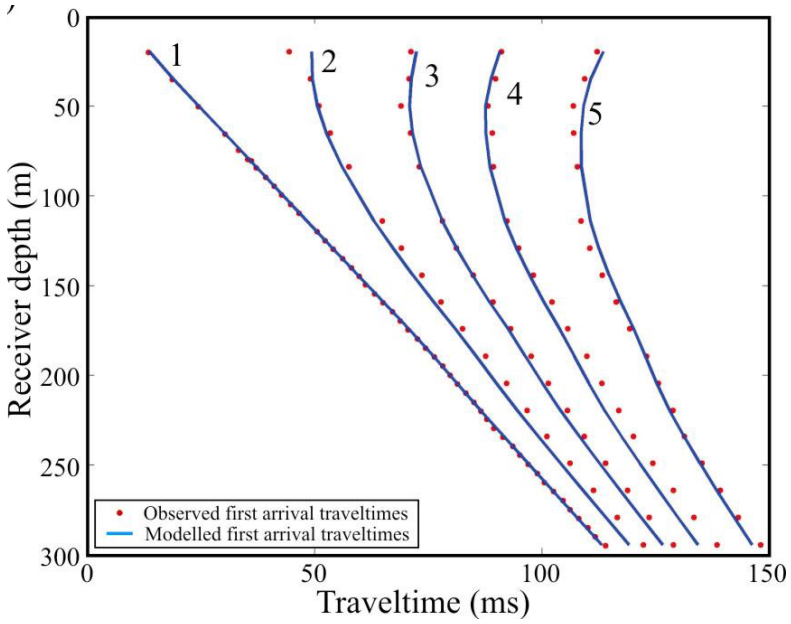

FIG. 9. Observed and calculated first-arrival P-wave traveltimes for walk-away shots in the Cygnet VSP survey.

The final model, used to generate the calculated times shown in Figure 9, is displayed in Figure 10. Velocity anisotropy was included in the model to determine whether the fit could be improved and a parameter scanning approach was used to evaluate effects of velocity anisotropy on computed first-arrival traveltimes. It was found that even with small values of ε and δ (0.03) in the two uppermost layers the match between computed and observed traveltimes was slightly superior only for the longest offset.

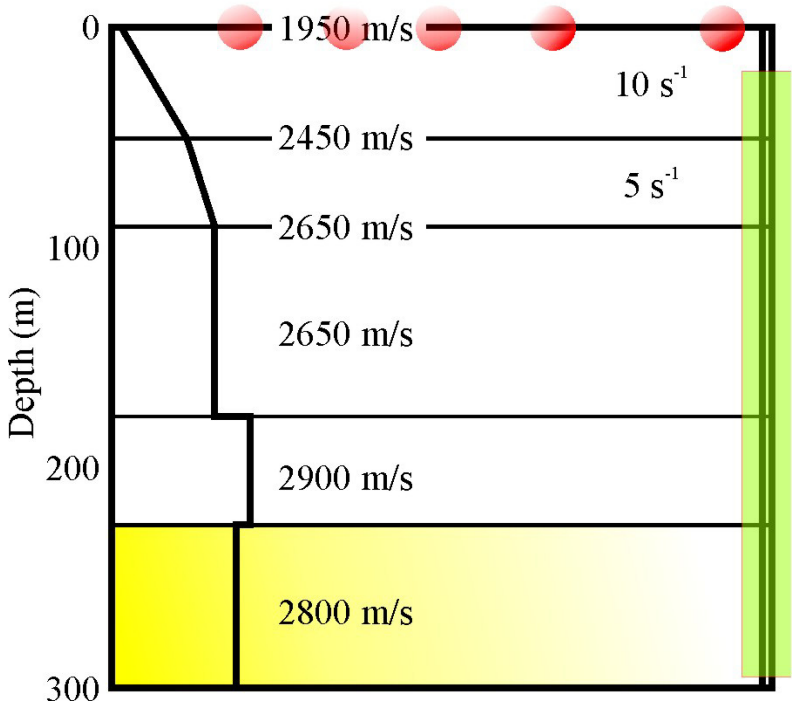

FIG. 10. Final P-wave velocity and depth model based on analysis of P-wave data from the Cygnet VSP.

WALKAWAY DIRECT S-WAVE DATA ANALYSIS

Processed VSP reflection data recorded from the four walk-away shots was reported by Richardson and Lawton (2003b). High quality VSP-CDP and VSP-CCP images were obtained of the Ardley for distances of up to 100 m from the well for the P-P data and 60 m for the P-S data. Examination of the raw data after rotation into the source-receiver plane showed high-amplitude events that are interpreted to be direct S-wave arrivals.

Rotated data with AGC scaling for display are shown in Figure 11. A point of interest was the polarity of the radial component after rotation. Standard industry practice (M. Jones, personal communication) is that the polarity of the radial component is assigned by have the polarity of the first arrival be the same as the polarity of the first arrival of the vertical component. For turning rays, this would result in the radial component changing polarity at the slowness cross-over depth, which would be incorrect. The rotation algorithm developed for this project ensured consistent polarity for the radial component, as seen in Figure 11. High amplitude SV-waves are visible on the vertical component

(weaker on the radial component data), and SH events are interpreted on the transverse component.

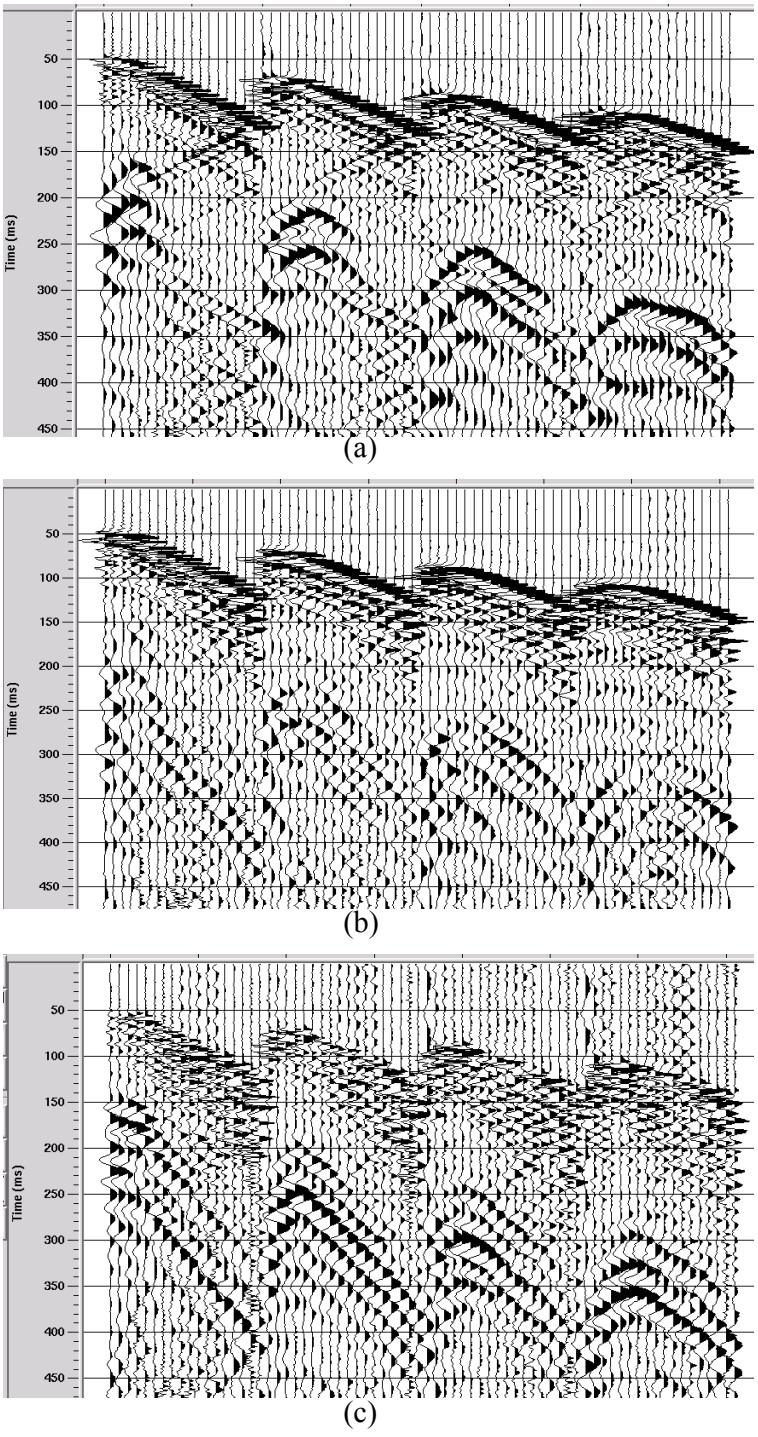

FIG. 11. Walkaway data after rotation. (a) vertical component; (b) radial component; (c) transverse component. Scaling (agc) has been applied for display. Source offsets increase for each panel from left to right in the displays.

Because of the clear SV data on the vertical component, this event was selected to examine the SV shallow velocity structure, using an identical procedure that used for the direct P-wave arrivals. Turning rays are interpreted for the SV waves, evidenced by the lack of monotonic moveout in the first arrival traveltimes versus depth and the polarity relationships about the SV-wave slowness cross-over depth (no change in the vertical component, but a polarity change in the radial component). An initial S-wave velocity model was developed from the zero-offset S-wave data and raytracing was undertaken to match calculated and observed direct S-wave arrivals from the three farthest source offsets. The 100 m offset data were excluded from the analysis because direct SV arrivals were difficult to pick at deeper receivers.

Interative modelling for the isotropic model with a range of gradients yielded a reasonable match between observed and calculated SV traveltimes. The best match for this model is shown in Figure 12. The fit is good for the far offset source, but the error increases for the two closer sourcepoints.

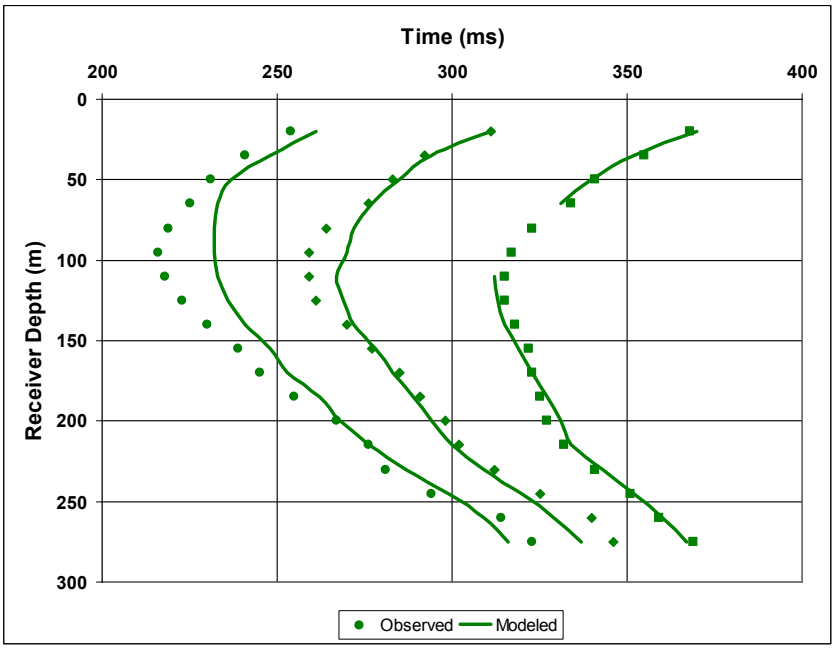

FIG. 12. Match between observed and calculated direct SV-arrivals for isotropic model.

The optimum model for the SV-velocity structure is shown in Figure 13. Vertical gradients of up to 18 s^{-1} were included in the model. The average vertical velocities were constrained by the zero-offset S-wave data, but the final model in Figure 13 is probably non-unique.

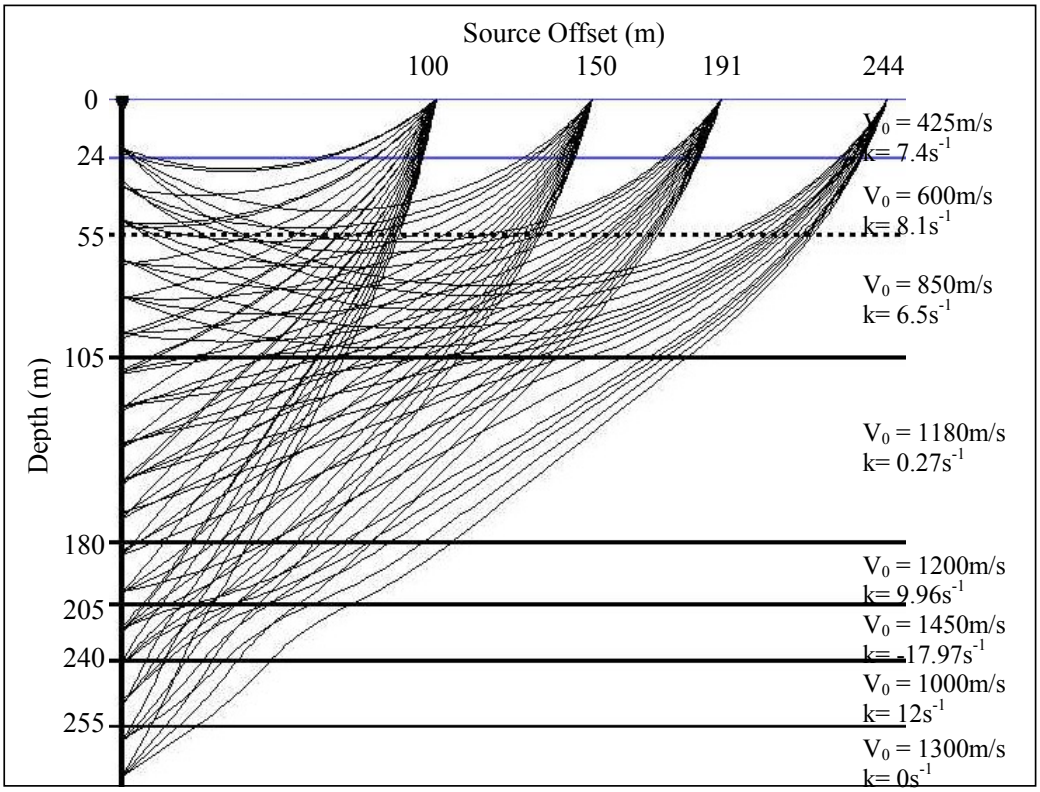

FIG. 13. Final SV velocity model and example raypaths.

Both the final P-wave and SV-wave velocity models were assessed by determining the incident angle of the direct arrival energy at the well, and comparing these observed angles with those calculated from raytracing. Figure 14 shows the match between the observed and calculated incident angles for the direct P-wave arrivals at source offsets of 150 m, 191 m and 244 m. The fit is good for the source offset of 150 m, and the calculated incident angles are slightly less than those observed for the 191 m and 244 m source offsets; i.e. the raytracing shows greater ray bending deeper in the model.

The match between the observed and calculated incident angles for the direct SV data are quite good at all source offsets, as shown in Figure 15, supporting the SV velocity model derived from traveltime inversion.

DISCUSSION AND CONCLUSIONS

Numerical modelling was used to successfully match calculated and observed first arrival traveltimes for the VSP recorded at Cygnet, Alberta. The presence of negative vertical apparent slowness values and reverse polarity first arrivals at shallow receivers in the borehole are diagnostic of vertical velocity gradients in the model.

An isotropic solution was found to match the observed and calculated first-arrival traveltimes well after interative tests using a parameter scanning approach. The final model consisted of five layers with vertical velocity gradients in the two uppermost layers of 10 s^{-1} and 5 s^{-1}, respectively. When anisotropy parameters $\varepsilon = 0.02$ and $\delta = 0.02$

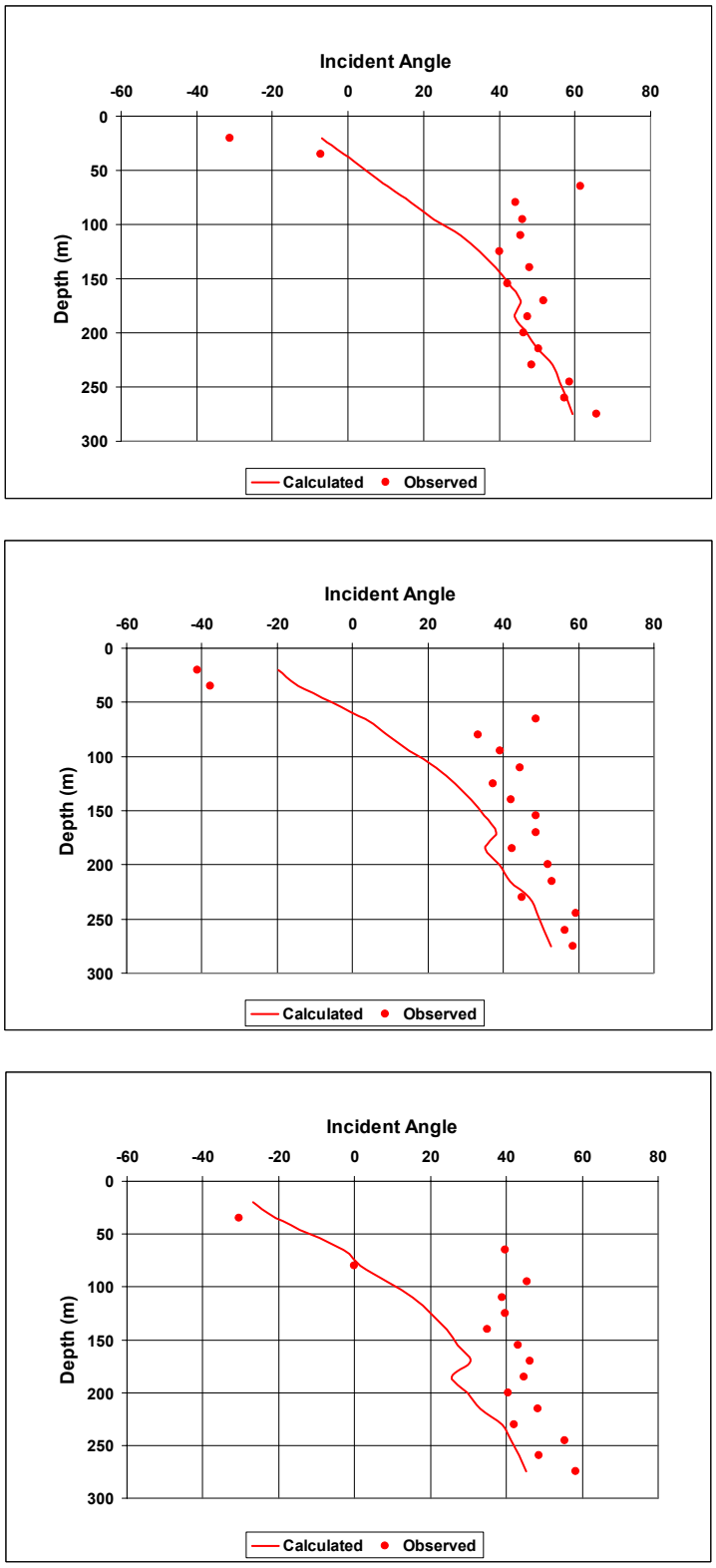

FIG. 14. Calculated and observed incident angles for P-waves at well for source offsets of 150 m (top), 191 m (centre) and 244 m (bottom).

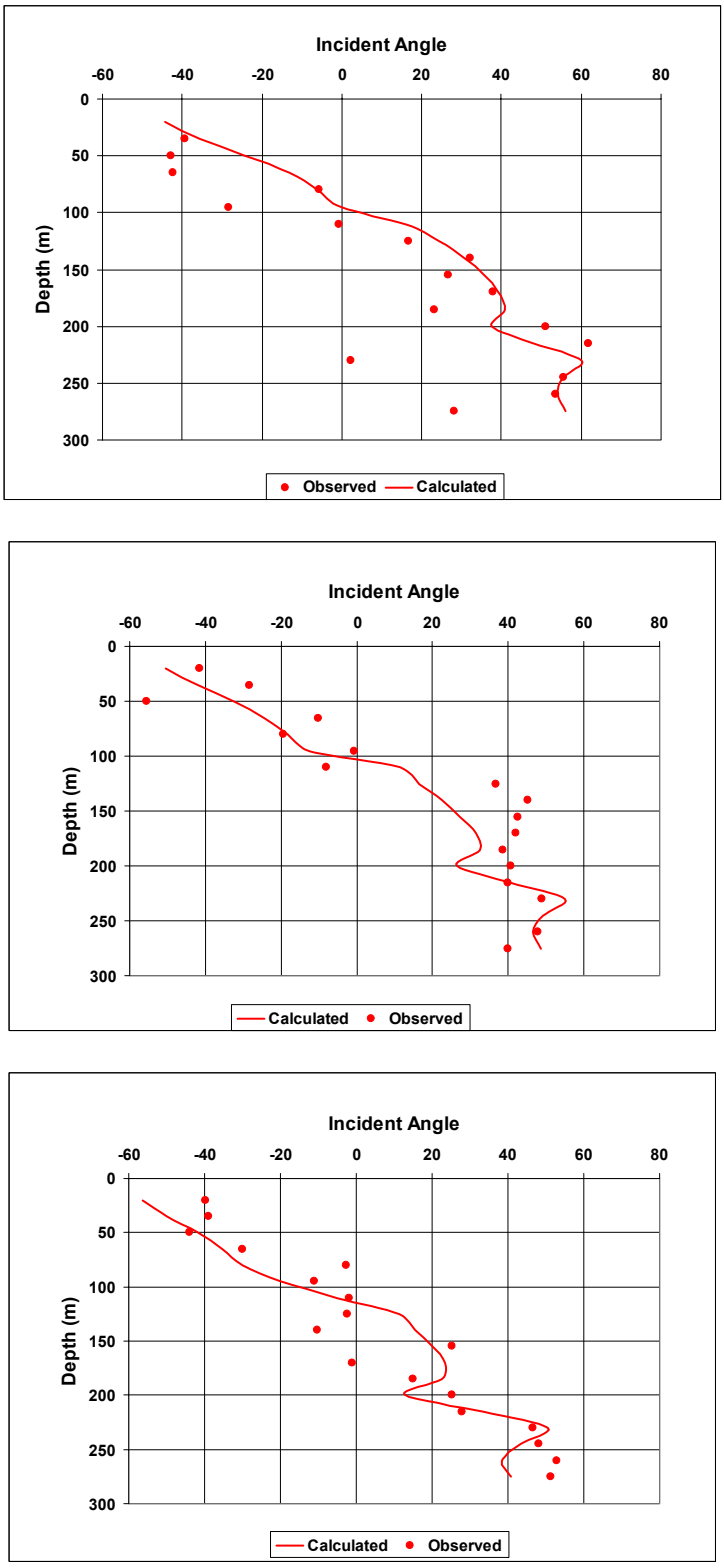

FIG. 15. Calculated and observed incident angles for SV waves at well for source offsets of 150 m (top), 191 m (centre) and 244 m (bottom).

were included in the two upper layers of the model, then a better match was found for the long offset near-surface traveltimes. For higher values of the anisotropy parameters, the resultant match was inferior.

The vertical minivibe source generated observable SV and SH energy that was recorded in the VSP data. Traveltime analysis of the first arrival SV data yielded an SV velocity model that included large vertical gradients, up to 18^{-1} in some of the near-surface layers.

Incident angle analysis of the recorded data was used to verify the velocity models interpreted from the traveltime analysis. The fit between observed and calculated incident angles at the well for the SV-wave data was very good, and reasonably good for the P-wave data.

ACKNOWLEDGEMENTS

We thank NSERC, the Alberta Energy Research Institute (AERI) and the sponsors of CREWES for supporting this research, as well as the industry partners who provided access to the Cygnet well for these experiments. Ms. Richardson was supported by and Alberta Ingenuity Fund Scholarship and Ms. Newrick was supported by the Fold-fault Research Project (FRP) at the University of Calgary. We also thank GX-technology for the use of Earthwave software for the raytrace modelling, and Landmark Graphics Corporation for the use of ProMAX.

REFERENCES

Beaton, A., 2003. Production potential of coalbed methane resources in Alberta, Energy & Utilities Board/Alberta Geological Survey Earth Sciences Report 2003-03, 68 pp.

Richardson, S.E., and Lawton, Don C., 2003a, Zero-offset vertical seismic profiles of coalbed methane strata: a comparison of three vibrating sources. CREWES Research Report, **15**.

Richardson, S.E., and Lawton, Don C., 2003b, PP and PS imaging and reflectivity of the Ardley coal zone, Red Deer, Alberta. CREWES Research Report, **15**.